JOURNAL OF SOLID STATE CHEMISTRY **131,** 121–130 (1997)
ARTICLE NO. SC977364

Spreading and Phase Transformations in Highly Dispersed CeO_2/SiO_2 and $Pd/CeO_2/SiO_2$ Systems

Leszek Kępiński[1] and Marek Wołcyrz

Institute of Low Temperature and Structure Research, Polish Academy of Sciences, P.O. Box 937, 50-950 Wrocław, Poland

Received September 5, 1996; in revised form February 20, 1997; accepted February 26, 1997

The effect of Pd on spreading and reaction of CeO_2 nanocrystallites with silica support on high temperature reduction in hydrogen was studied by X-ray diffraction (XRD), high resolution transmission electron microscopy (HRTEM), and selected area electron diffraction (SAED). Without Pd, CeO_2 nanocrystallites (size ca. 5 nm) began to spread onto the silica at 870 K, producing at 970 K uniform nearly amorphous overlayer. With Pd, the spreading occurred at 100 K lower temperature and moreover at 970 K the raft-like $Ce_{4.67}(SiO_4)_3O$ silicate crystals were formed in contact with the Pd particles. Chlorine from the $PdCl_2$ precursor reacted with ceria at 770 and 870 K to form the ribbon-like CeOCl crystals, which at 970 K became unstable, probably undergoing transformation into Ce silicate. Formation of Ce silicate and CeOCl during the high temperature reduction is a possible mechanism of the deactivation of the ceria-promoted Pd/SiO_2 catalysts (irreversible Ce^{4+} to Ce^{3+} reduction).

INTRODUCTION

Highly dispersed, monomolecular layers of active oxides deposited on the surface of an inert support have been intensively studied for many years, mainly due to their applications as catalytic systems (1). The dispersed oxide may constitute itself the catalytically active phase as it happens in the V_2O_5 base systems (2) or eventually it may act as a promoter, modifying the properties of the main active phase, e.g., the metal catalyst. Noble metal catalysts promoted with cerium oxide have gained considerable interest in recent years because of their successful application in the exhaust gas control and in the Fischer–Tropsch synthesis. In particular, $Me/CeO_2/SiO_2$ catalysts were studied to elucidate the mechanism of promoting effect of Ce in the reactions of CO and CO_2 hydrogenation (3–7). It has been postulated that the decoration of Pd by CeO_x moieties (3), the presence of Ce^{3+} ions on the surface of Rh particles inducing the electronic interactions (4, 5), and the existence of the surface oxygen vacancies at the Rh/ceria interface (7) are responsible for an improved selectivity of the promoted catalyst. Detailed TEM and XRD studies revealed that in the $Me/CeO_2/SiO_2$ systems the strong chemical interactions occur during the reduction treatment at high temperatures (7–9). For $Rh/CeO_2/SiO_2$ thin film samples, the extensive studies of Krause *et al.* (8) revealed complex microstructure transformations involving the spreading of CeO_2 on SiO_2 with eventual formation of cerium silicate catalyzed by Rh. Kępiński and Wołcyrz (9) also reported the spreading of CeO_2 on high surface SiO_2 on heating in hydrogen at 870 K, with a slight promoting effect of Pd. Recently, Trovarelli *et al.* (7) reported CeO_2 redispersion in $Rh/CeO_2/SiO_2$ high surface samples during the reduction at 773 K and again with the promoting effect of Rh.

In this work we studied the effect of Pd and chlorine from its precursor on the spreading of CeO_2 nanocrystals ($\sim$5 nm) on a surface of amorphous SiO_2 during high temperature reduction in hydrogen. In particular we focused attention on the role of Pd particles as possible nucleation centers of the CeO_2–SiO_2 reaction leading eventually to the formation of cerium silicates. Since the reaction is likely to be limited to a very thin surface layer (8) we used HRTEM as the most suitable experimental tool. Information on the overall phase composition of the samples was obtained by XRD.

EXPERIMENTAL

SiO_2 support used was Rhone–Poulenc XOB-15 silica with a specific surface of 35 m^2/g. The support was impregnated with an appropriate amount of a 20 wt% colloidal suspension of CeO_2 (Aldrich) to get 30 wt% CeO_2/SiO_2 composition. The slurry was dried overnight in air at 350 K and finally ground in a mortar. Pd (1 wt%)/30 wt% CeO_2/SiO_2 sample was prepared by impregnation of the CeO_2/SiO_2 powder with an appropriate amount of $PdCl_2$

[1] To whom correspondence should be addressed. E-mail: kepinski@highscreen.int.pan.wroc.pl.

0022-4596/97 $25.00

solution. Then the sample was dried and ground. Reduction of the samples was performed in a hydrogen flow at 1 atm at 770, 870, and 970 K for 20 h. Then the hydrogen was pumped off and the samples were cooled to room temperature in vacuum of ca. 10^{-5} Torr. This procedure assured that no hydrides were left in the samples. The hydrogen was purified by passing it over a Pd/asbestos catalyst kept at 450 K, NaOH, and finally P_2O_5.

Evolution of a microstructure of the samples was studied *ex situ*, after their exposure to air, by X-ray diffraction (Stoe powder diffractometer, Cu$K\alpha$ radiation), high resolution transmission electron microscopy (HRTEM), and selected area electron diffraction (SAED) (Philips CM20 SuperTwin). To the samples studied by XRD 40 wt% of corundum (α-Al_2O_3) powder was added as an internal standard to allow for the determination of the true peak positions and widths and also the amounts of crystalline phases present. Average crystallite size of the phases was calculated from the XRD spectra by using the Scherrer formula: $L = \lambda K/B_0 \cos\Theta$, where λ is the wavelength of radiation (0.154 nm), K is a constant (0.9), and B_0 is the width of the peak at 2Θ corrected for the instrumental broadening. Samples for TEM and ED were prepared by dispersion of some powder in absolute ethanol and putting a droplet of the suspension on a copper microscope grid covered with perforated carbon.

RESULTS

XRD

Figure 1 and Table 1 show XRD results for CeO_2/SiO_2 (Fig. 1a) and $Pd/CeO_2/SiO_2$ (Fig. 1b) samples reduced at various temperatures. In the CeO_2/SiO_2 sample only peaks of CeO_2 and corundum standard are seen (SiO_2 is amorphous and does not produce any visible peaks in the 2Θ range studied), but with increasing temperature ceria peaks broaden and decrease in intensity to nearly zero at 970 K. Splitting of the CeO_2 peaks at 870 K indicates its partial reduction to the oxygen-deficient CeO_{2-x} phase with an expanded lattice parameter (10, 11).

The $Pd/CeO_2/SiO_2$ sample exhibits more complex behavior. Nearly complete amorphization of ceria takes place already at 870 K, i.e., 100 K below the temperature for the CeO_2/SiO_2. Moreover, at 770 K peaks from a new phase become visible at $2\theta = 25.4°$ (superimposed on corundum peak), 30.92°, 34.14°, and 44.4°. The peaks increase in

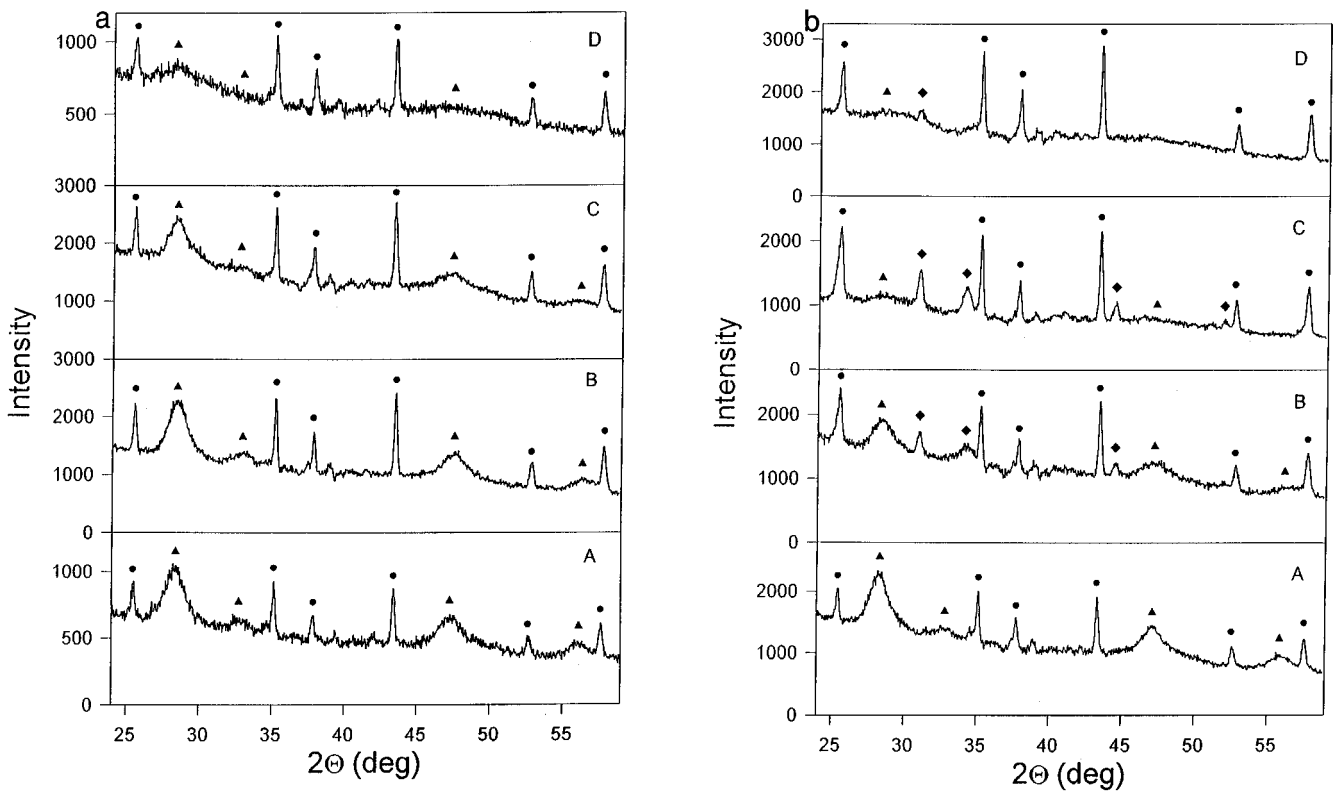

FIG. 1. XRD spectra of CeO_2/SiO_2 (a) and $Pd/CeO_2/SiO_2$ (b) samples "as prepared" (A) and heated in hydrogen at 770 K (B), 870 K (C), and 970 K (D) for 20 h. Peak assignment: CeO_2 (▲), CeOCl (◆), corundum (α-Al_2O_3) standard (●).

TABLE 1
Summary of XRD Data for CeO_2/SiO_2 and $Pd/CeO_2/SiO_2$ Samples Heated in Hydrogen

Sample	Al_2O_3 113 (43.36°)		CeO_2 111 (28.4°)			CeOCl 110 (30.92°)		CeOCl 102 (34.14°)		R^a
	B	I^b	$B_0{}^c$	I	L^d	B_0	I	B_0	I	
					CeO_2/SiO_2					
no	0.24	137	1.55	814	5.8					5.94
770 K	0.22	442	1.48	1784	6.2					4.04
870 K	0.23	465	1.43	1242	6.4					2.67
970 K	0.25	180	3.30	410	2.8					2.28
					$Pd/CeO_2/SiO_2$					
no	0.22	272	1.55	1756	5.8	—	—	—	—	6.45
770 K	0.23	371	1.63	995	5.5	0.30	193	1.25	463	2.68
870 K	0.24	452	3.22	448	2.8	0.30	309	0.69	424	0.99
970 K	0.21	539	—	—	—	0.40	134	—	—	—

[a] $R = I(CeO_2)/I(Al_2O_3)$.
[b] Intensity of the peak.
[c] Width (FWHM) of the peak corrected for the instrumental broadening (°).
[d] Average crystallite size (nm).

intensity at 870 K and then nearly disappear at 970 K. We identified this phase before in Pd/CeO_2 catalyst prepared from $PdCl_2$ as tetragonal CeOCl (10, 12). A large difference in the widths of various CeOCl peaks is evident (Fig. 1b); the 102 peak at 34.14° is twice as broad as the 110 peak at 30.92° (see Table 1). The TEM study showed (see below) that this is the result of the particular, ribbon-like shape of the CeOCl crystallites.

TEM

Figure 2 shows the microstructure of the "as prepared" CeO_2/SiO_2 sample. In Fig. 2a bright field (BF) and dark field (DF) images of the same area are presented (DF image is formed by electrons diffracted into a portion of a CeO_2 (111) ring). CeO_2 crystallites that are under the proper diffraction conditions appear as white dots in the DF image and their average size and distribution on the support can be analyzed. It is seen that the typical crystallite size is 3–7 nm, and the crystallites are rather uniformly distributed on the silica surface. The SAED pattern (inset in Fig. 2a) contains only rings of cubic CeO_2 and a very broad innermost ring from an amorphous silica. In the high resolution image (Fig. 2b) CeO_2 crystallites can be discriminated as patches of parallel lattice fringes with a distance of 0.32 nm (CeO_2 (111) lattice planes). Crystallites with the typical size 3–7 nm are seen to form aggregates of various sizes.

Only minor changes in the microstructure were detected after heating the sample in hydrogen at 770 K and at 870 K but at 970 K drastic modifications occurred (Fig. 3a). The edges of silica grains became smoother and the average size of CeO_2 crystallites decreased so that a nearly uniform layer of extremely small "crystallites" (below 1 nm) is present on the surface of silica (the layer is visible particularly well at the edge of silica grains, where it is imaged as a side view). The HRTEM image of this sample (Fig. 3b) shows, however, that in the bulk of ceria aggregates there are still areas of crystalline CeO_2.

Micrographs of the "as prepared" $Pd/CeO_2/SiO_2$ sample were very similar to those of the CeO_2/SiO_2 sample (Fig. 2). Thermal evolution of the microstructure of the doped sample generally reflected that of CeO_2/SiO_2 but important microstructure changes occurred at temperatures ca. 100 K lower. At 870 K there are practically no CeO_2 crystallites visible in BF and DF images and also only very diffuse rings of ceria are seen in the SAED pattern (Fig. 4a). However, in the SAED pattern of the sample heated at 870 K (and also at 770 K) numerous sharp reflections from a new crystal phase are seen (Fig. 4a). In the high resolution image (Fig. 4b) crystals of this phase are visible as ribbon-like objects exhibiting strong 0.68 nm lattice fringes parallel to the ribbon plane. The morphology of the crystals is characteristic for cerium oxychloride, CeOCl (10). No significant change in the general appearance of the sample occurred after heating at 970 K, except for reduction in the number of CeOCl crystals and occurrence in the DF image of relatively large crystalline patches of another new phase. Interestingly, the SAED pattern contains only very broad rings suggesting an amorphous structure. Close inspection of the sample by HRTEM revealed, however, that crystals of a new crystalline phase are sometimes visible in contact with Pd particles.

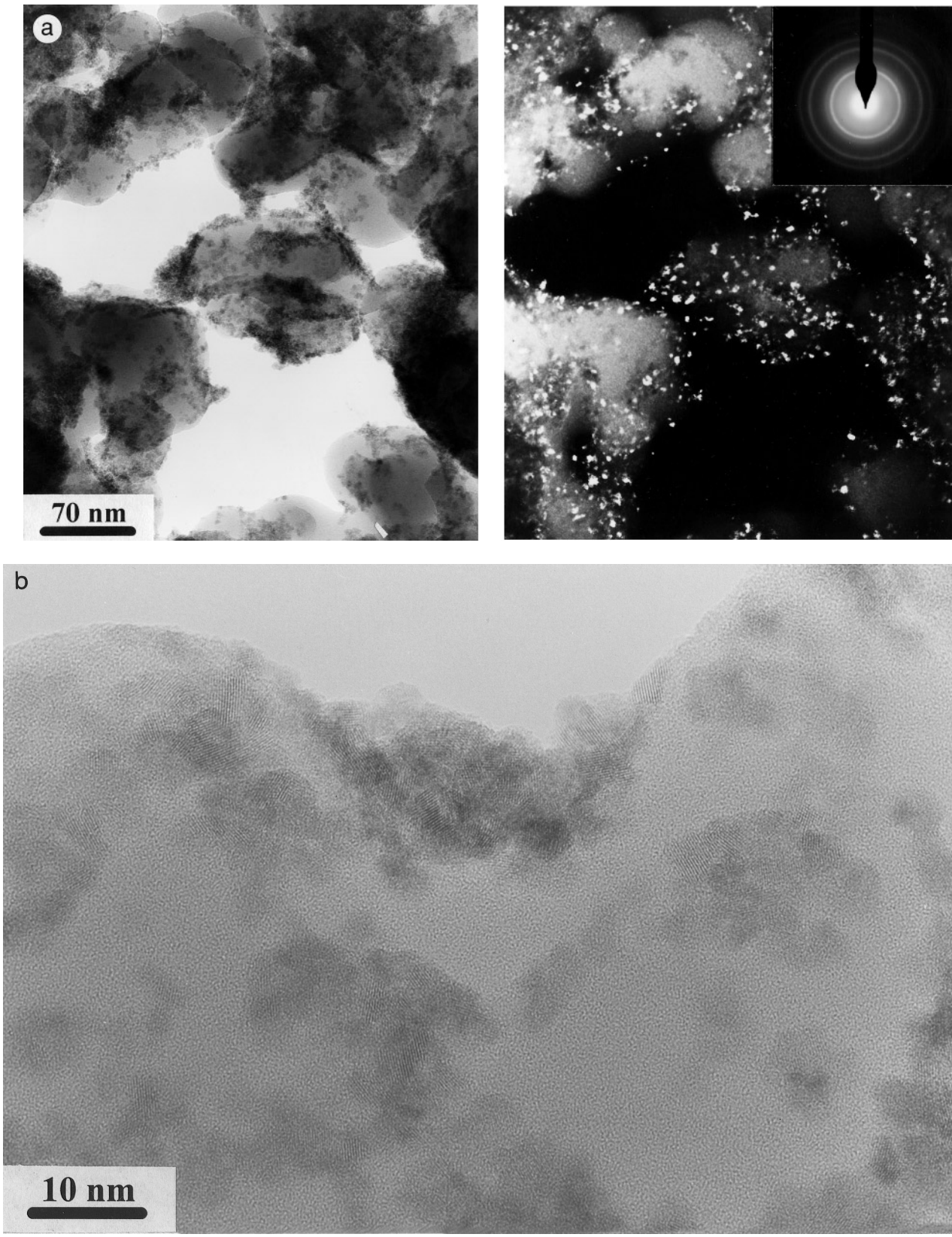

FIG. 2. Microstructure of the "as prepared" CeO_2/SiO_2 sample. Bright field (BF) dark field (DF) images and SAED pattern (a) and HRTEM image (b) are shown.

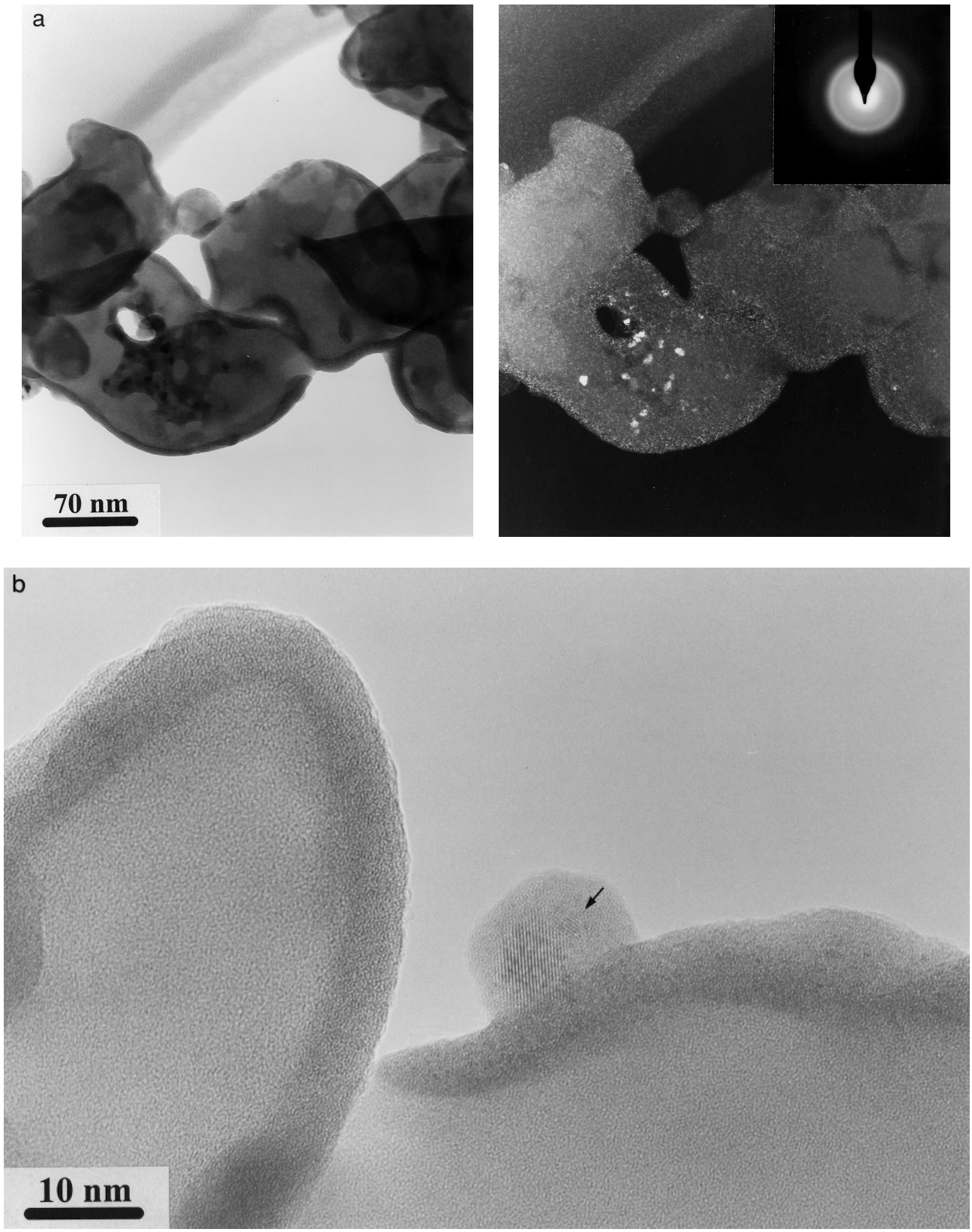

FIG. 3. Microstructure of the CeO_2/SiO_2 sample heated in hydrogen at 970 K. BF, DF images and SAED pattern (a) and HRTEM image (b) are shown. Note the occurrence of a crystalline CeO_2 inside the ceria grain in (b).

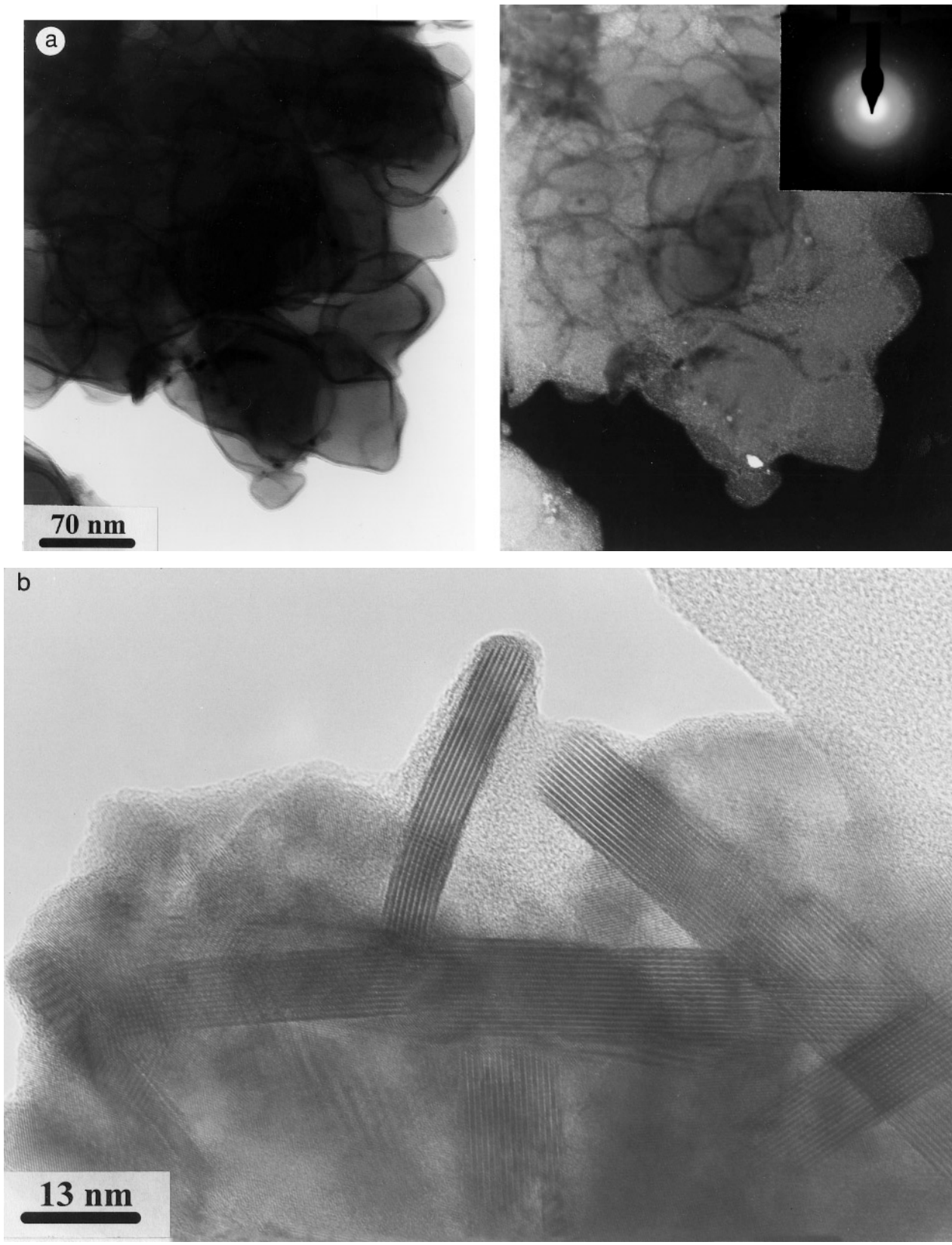

FIG. 4. Microstructure of the $Pd/CeO_2/SiO_2$ sample heated in hydrogen at 870 K. BF, DF images and SAED pattern (a) and HRTEM image (b) are shown. Note the occurrence of the ribbon-like CeOCl crystals in (b).

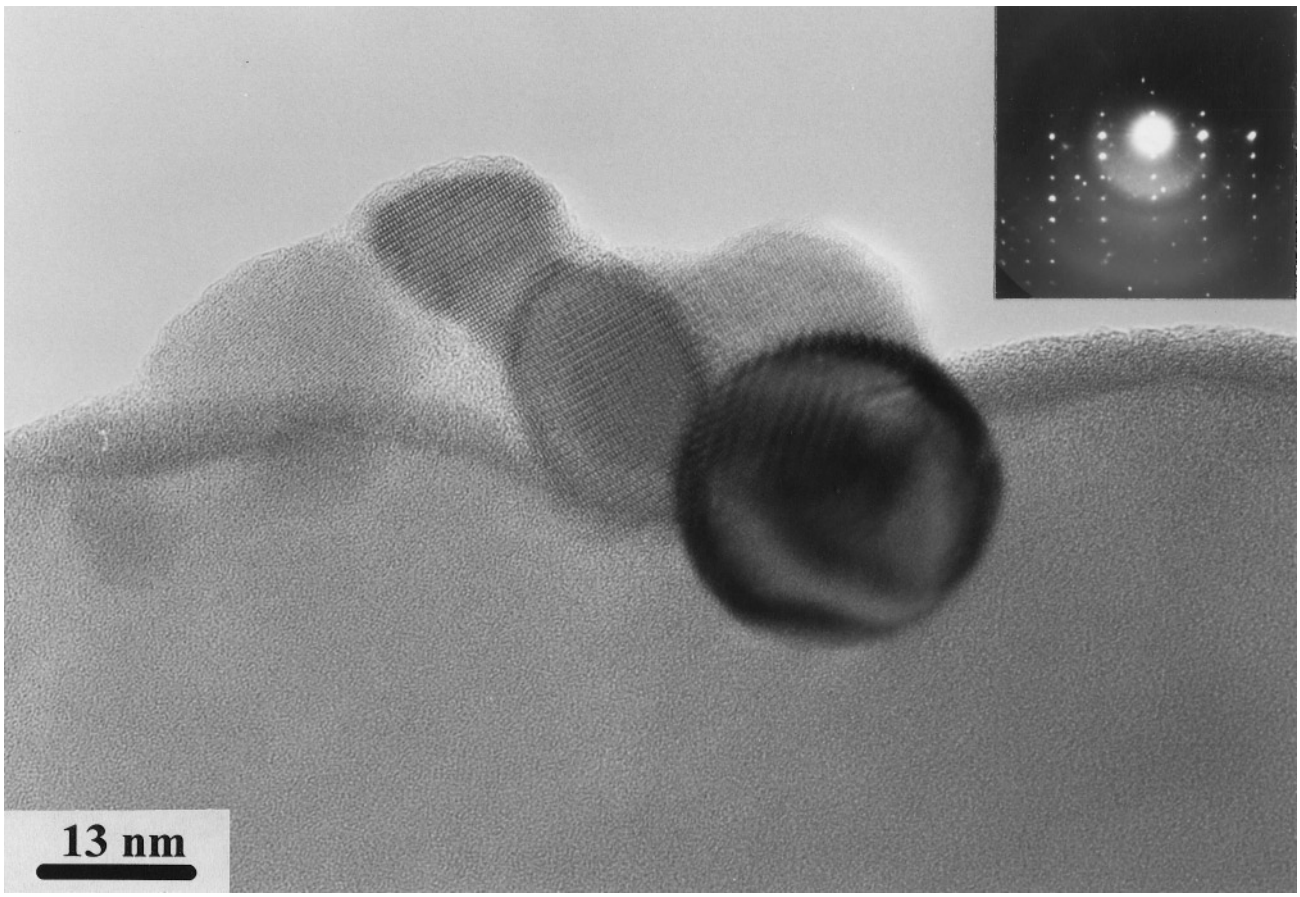

FIG. 5. HRTEM image of the $Pd/CeO_2/SiO_2$ sample heated at 970 K. Note well aligned crystal of the new phase in contact with Pd particle (dark).

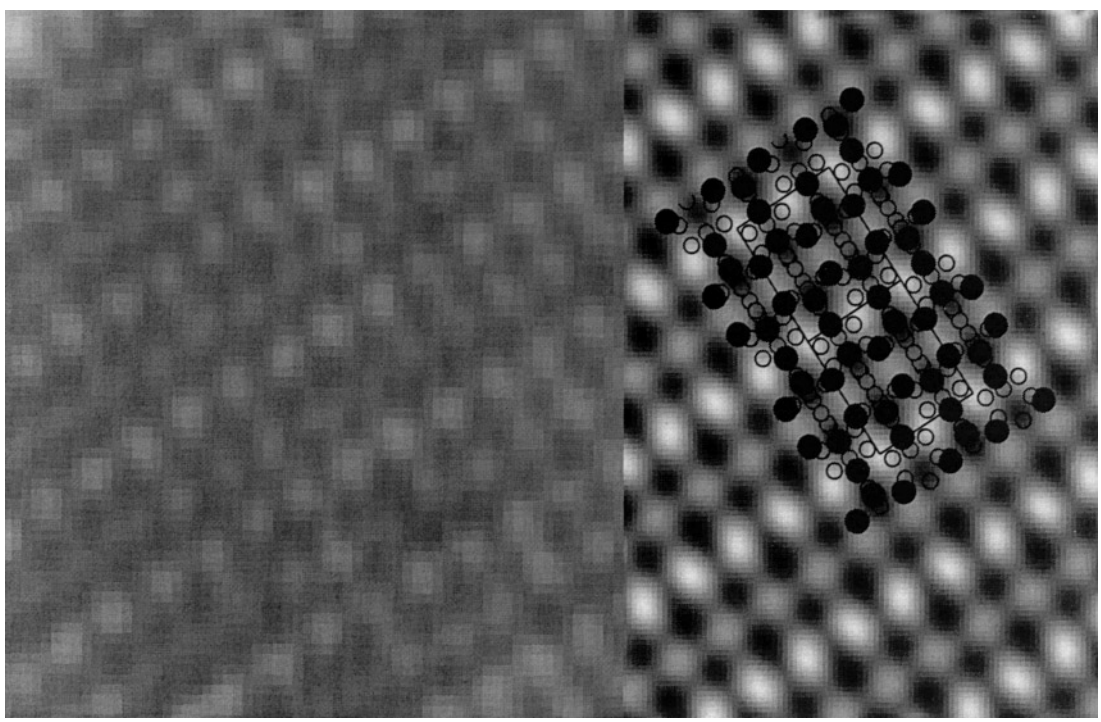

FIG. 6. Crystallographic image processing of the image of the crystallite from Fig. 5. Magnified original image and filtered image are shown. As inset the [110] projection of the hexagonal $Ce_{4.67}(SiO_4)_3O$ is included (black dots – Ce atoms, empty dots – O and Si atoms).

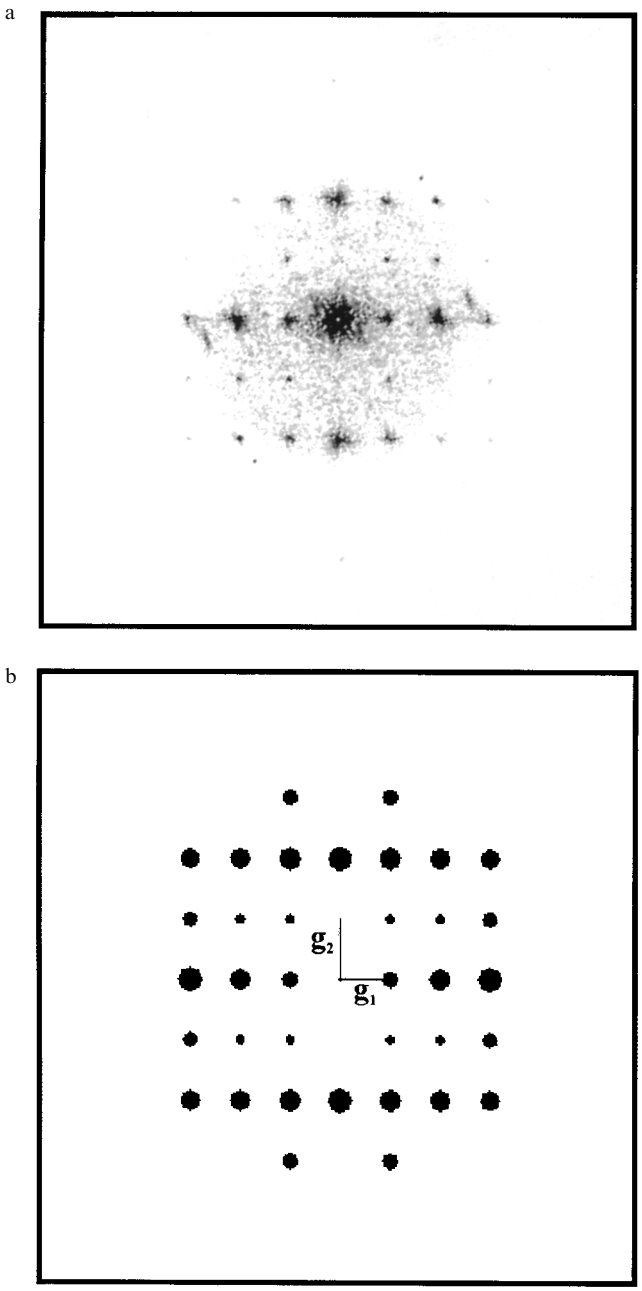

FIG. 7. Comparison of the FFT pattern of the original image (a) and theoretical, dynamical electron diffraction pattern calculated for the $Ce_{4.67}(SiO_4)_3O$ in [110] orientation (b). In (b) $g_1 = (1\ -1\ 0)$ and $g_2 = (0\ 0\ 1) = \mathbf{c}^*$.

Figure 5 shows an example of a crystal in a zone axis orientation. The crystal is 50 nm long and is attached to a 26 nm diameter Pd particle. The SAED pattern of the crystal (Fig. 5) could be indexed in rectangular lattice with $a = 0.84$ nm and $c = 0.71$ nm.

Application of a crystallographic image processing (CIP) procedure (CRISP package (13)) to a fragment of the HRTEM image in Fig. 5 (thin region of a top-left crystallite) allowed us to determine a two-dimensional lattice cell (rectangular: $a = 0.84$ nm, $b = 0.71$ nm) and the most probable plane group (*pmg*). The results of the image processing are shown in Fig. 6 where original and filtered (symmetry corrected) images are compared. As an inset in Fig. 6 a [110] projection of a crystal structure of the hexagonal $Ce_{4.67}(SiO_4)_3O$ silicate ($a = 0.9736$ nm, $c = 0.7116$ nm, space group $P6_3/m$ (14)) is included (large black dots represent Ce atoms, while small empty dots represent O and Si). Projection of the lattice cell of the silicate (rectangle with dimensions 2×0.843 nm and 0.7116 nm) fits our CIP results very well. In Fig. 7, FFT (Fast Fourier Transform) of the original image is shown (a) and compared with the dynamical electron diffraction pattern calculated for the $Ce_{4.67}(SiO_4)_3O$ structure with the EMS software (15). In both cases systematic absences occur on the $(0, k)$ line for $k = 2n + 1$ indicating the *pg* or *pmg* plane group. The [110] projection of the $Ce_{4.67}(SiO_4)_3O$ (cf. Fig. 6) also exhibits *pmg* symmetry (the *g* plane is parallel to **c** axis). These observations and the fact that no other compound that could form under our experimental conditions fits our data allow us to believe that the $Ce_{4.67}(SiO_4)_3O$ grows as the result of a ceria–silica reaction in hydrogen. Figure 8 shows two HRTEM images of another crystallite of the new phase taken at small tilt ($\sim 15^\circ$). Lattice fringes (0.84 nm) visible in both images are at 60° to each other, matching well the (100) and (010) planes of the hexagonal $Ce_{4.67}(SiO_4)_3O$. It appears that the crystallite is oriented with the **c** axis close to the beam direction and thus its (001) crystal plane is probably parallel to the surface of the silica grain. Figure 8 shows also that the (100) and (010) fringes extend far away from the Pd particle (ca. 80 nm) and that their contrast is quite weak. We expect therefore that the crystallite must be very thin, which explains why this phase gives very weak reflections in SAED patterns and no peaks in XRD spectra. It is worth noting also that apparently the $Ce_{4.67}(SiO_4)_3O$ crystals grow only in contact with the Pd particles (cf. Figs. 5 and 8).

DISCUSSION

Results presented in this work are consistent with earlier findings that in hydrogen ceria wets SiO_2 at or above 870 K producing an amorphous overlayer on its surface (6–9). We showed that 30 wt% of CeO_2 deposited as fine crystallites (ca. 5 nm) on high surface silica underwent complete amorphization at 973 K, while Krause *et al.* (8) observed the same effect at 870 K for 2 nm thick ceria film evaporated on a flat silica. In both cases a multilayer amorphous structure was formed. Trovaralli *et al.* (7) found only partial amorphization of CeO_2 crystallites (ca. 13 nm average size) at 773 K for high CeO_2 loading (28.4 wt%), but complete amorphization at low CeO_2 loading (1.6 wt%). It appears

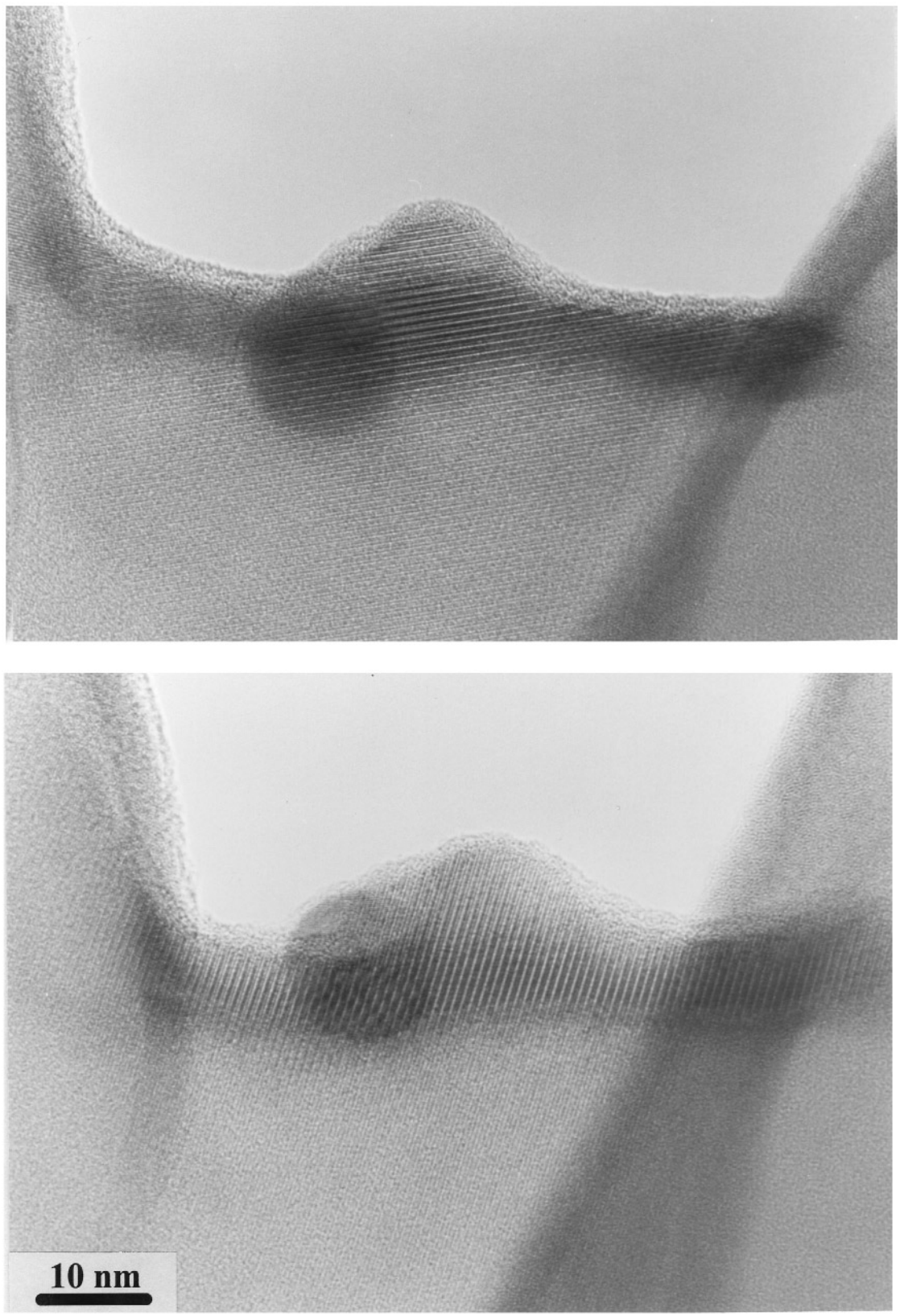

FIG. 8. HRTEM images of a crystallite of the silicate phase taken at small tilt (15°). Note the occurrence of 0.84 nm fringes at 60° to each other and their extension far away from Pd particle (dark).

that important factors determining efficient spreading of CeO_2 on SiO_2 are the small size of ceria crystallites and the high contact area between the oxides.

An important question concerns the chemical state of cerium atoms in the amorphous layer on silica. Krause *et al.* (8) gave evidences that Ce is present mostly as Ce^{3+}, i.e., having stoichiometry close to Ce_2O_3. However, some intermixing with silica resulting in formation of an amorphous "silicate" may not be excluded. Presence of the metal particles (Rh (7, 8) or Pd (9, this work)) facilitates the CeO_2 amorphization, but also "catalyzes" nucleation and growth of thin, crystalline Ce silicate (8, this work). There is, however, a discrepancy between results of (8) and ours. We identified the silicate as the hexagonal $Ce_{4.67}(SiO_4)_3O$ contrast to the orthorhombic $Ce_2Si_2O_7$ proposed in (8). A recent XRD study on compound formation in the ceria–silica system in reducing atmosphere ($H_2 + N_2$) (16) seems to support our data. The hexagonal $Ce_{4.67}(SiO_4)_3O$ was observed as the first silicate phase at 1270 K, while the orthorhombic $Ce_2Si_2O_7$ phase occurred as the last one at 1670 K (16). We believe that our observation of the $Ce_{4.67}(SiO_4)_3O$ formation already at 970 K, i.e., 300 K below the temperature reported in (16), is the result of using a much more sensitive detection tool, HRTEM (it should be remembered that we did not observe silicate phase in the XRD spectra), and also the "catalytic" action of palladium particles.

In this work we showed also that in the $Pd/CeO_2/SiO_2$ system prepared from $PdCl_2$ precursor, similarly to the Pd/CeO_2 catalyst (10, 12), another crystalline phase containing Ce^{3+} ions, namely CeOCl, is formed at 770 K. There is, however, a difference between the two systems; in Pd/CeO_2 the CeOCl phase was stable at 970 K (10), but in the presence of SiO_2 it becomes unstable at this temperature and possibly transforms into more stable Ce silicate (see Fig. 1b). At moderate temperatures both Ce silicate and CeOCl are stable also in oxidizing atmosphere, which means that part of Ce^{4+} ions in the system is "irreversibly" reduced into the Ce^{3+} state and therefore cannot participate in the oxygen exchange process. This may be considered as one of the possible mechanisms of deactivation of Pd/SiO_2 catalysts promoted with ceria.

SUMMARY

1. We confirmed that in hydrogen CeO_2 nanocrystallites (5 nm) spread over a high surface silica support at 870 K. At 970 K uniform, a nearly amorphous ceria multilayer is formed (crystallite size below 1 nm). Addition of Pd (1 wt%) reduces the spreading temperature by 100 K.

2. Pd particles added to the CeO_2/SiO_2 system "catalyze" the nucleation of the crystalline $Ce_{4.67}(SiO_4)_3O$ silicate in hydrogen at 970 K. The silicate forms flat, raft-like objects oriented with the **c** axis perpendicular to the surface of silica grains.

3. Chlorine from $PdCl_2$ precursor reacts with the ceria overlayer in hydrogen starting at 770 K to form ribbon-like CeOCl crystals. At 970 K CeOCl starts to decompose, probably undergoing transformation into the cerium silicate.

4. Formation of cerium silicate and cerium oxychloride during high temperature reduction of the $Pd/CeO_2/SiO_2$ system is one of the mechanisms of the catalyst deactivation (Ce^{4+} is irreversibly reduced to Ce^{3+}).

ACKNOWLEDGMENT

The authors thank Mrs. Z. Mazurkiewicz for skillful assistance in the samples preparation and for the excellent photographic work.

REFERENCES

1. J. Haber, *Pure Appl. Chem.* **56,** 1663 (1984).
2. J. Haber, A. Kozłowska, and R. Kozłowski, *J. Catal.* **102,** 52 (1986).
3. J. S. Rieck and A. T. Bell, *J. Catal.* **99,** 278 (1986).
4. A. Kienneman, B. Raymond, J. P. Hindermann, and M. Laurin, *J. Chem. Soc., Faraday Trans.* **83,** 2119 (1987).
5. J. C. Lavalley, J. Saussey, J. Lamotte, R. Breault, J. P. Hindermann, and A. Kienneman, *J. Phys. Chem.* **94,** 5941 (1990).
6. T. Chojnacki, K. Krause, and L. D. Schmidt, *J. Catal.* **128,** 161 (1991).
7. A. Trovarelli, C. de Leitenburg, G. Dolcetti, and J. Llorca, *J. Catal.* **151,** 111 (1995).
8. K. R. Krause, P. Schabes-Retchkiman, and L. D. Schmidt, *J. Catal.* **134,** 204 (1992).
9. L. Kępiński, and M. Wołcyrz, *Catal. Lett.* **15,** 329 (1992).
10. L. Kępiński, M. Wołcyrz, and J. Okal, *J. Chem. Soc., Faraday Trans.* **91,** 507 (1995).
11. V. Perrichon, A. Laachir, G. Bergeret, R. Frety, L. Tournayan, and O. Touret, *J. Chem. Soc., Faraday Trans.* **90,** 773 (1994).
12. M. Wołcyrz, and L. Kępiński, *J. Solid State Chem.* **99,** 409 (1992).
13. S. Hovmoller, *Ultramicroscopy* **41,** 121 (1992).
14. E. L. Belokoneva, T. L. Petrova, M. A. Simonov, and N. V. Bielov, *Kristallografiya* **17,** 490 (1972).
15. P. H. Jouneau and P. Stadelmann, "EMS On-Line," Centre Interdepartemental de Microscopie Electronique, EPFL, Lausanne.
16. H. A. M. van Hal and H. T. Hintzen, *J. Alloys Comp.* **179,** 77 (1992).